Direct visualization of hollow fiber membrane fouling distribution

Petr Bílek[1,*], *Filicia Wicaksana*[2]

[1]Department of Nanotechnology and Informatics, Technical University of Liberec, Studentská 1402/2, 461 17, Liberec 1, Czech Republic[1]
[2]Department of Chemical and Materials Engineering, the University of Auckland, 2-6 Park Avenue, Grafton 1023, Auckland, New Zealand[2]

Abstract. Submerged membrane bioreactor system is commonly used for water and wastewater treatment processes. This system is a more economical alternative to conventional activated sludge process due to small footprint and better effluent quality. Nevertheless, membrane fouling is a major issue that requires further studies. This paper covers the use of an optical microscope to observe membrane fouling. Bentonite was used as model particles to simulate activated sludge. In-situ observation of particle deposition along the surface of hollow fiber membranes during filtration was performed at various operating conditions. Results from this studies indicated that the flux distribution was affected by the permeate flux and cross flow velocity. Lower CFV and higher flux caused the flux to be more non-uniformly distributed due to more severe fouling. These findings provided useful information to further improve the membrane module design to achieve more evenly distributed permeate flux.

1 Introduction

Membranes are widely used for various applications (wastewater treatment, drinking water production, food processing and pharmaceutical industry). Compared to flat sheet membranes, hollow fiber membranes offer higher packing density and higher mechanical strength since hollow fiber membranes are self-supporting. Hollow fiber membranes are commonly used in submerged membrane bioreactors for wastewater treatment. The fibers are arranged in parallel and directly immersed in a bioreactor. However, since the membranes are in direct contact with the mixed liquor, membrane fouling is inevitable. The deposition of foulants on the surface of fibers gradually reduces the permeate flow. There are several ways to reduce membrane fouling, such as back-flushing, back washing, the use of air bubbles to scour the membrane surface and ultrasound [1-2].
The small aspect ratio of hollow fiber membranes causes high axial pressure gradient inside the fibers and consequently, the flux gradient. In addition to this, the pressure gradient is also governed by the mode of operation. Submerged hollow fiber membranes are typically operated with the permeate extracted from the upper end of the module, while the other end is sealed. This leads to non-uniformity of permeate flux distribution. It is hypothesized that the highest flux would occur close to the permeate suction point and decrease towards the opposite (sealed) end (Figure 1). If the permeate is extracted from both ends of the fiber, the lowest flux would be in the middle of the fiber. It is expected that the fouling pattern mirrors the flux gradient: the higher the flux, the more severe the fouling.

* petr.bilek@tul.cz

A model was developed by Carroll, et al. [3] to correlate local permeate flux to fiber length and diameter. Results from their modelling study highlighted the presence of non-uniform axial flux profile that resulted in dynamic fouling patterns.

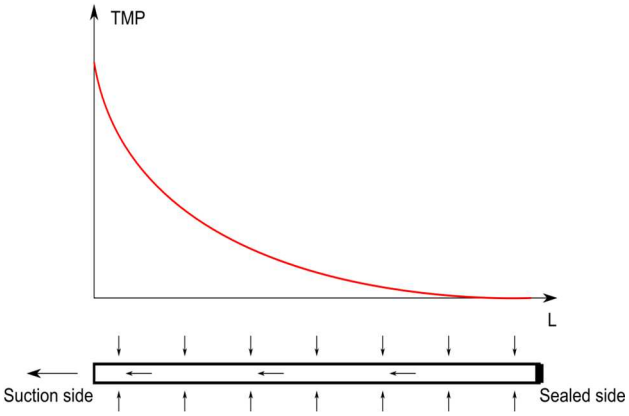

Fig. 1. TMP profile along a hollow fiber membrane.

The non-uniformity of local permeate flow was also reported by former researchers through a simulation study [4] and hollow fiber membrane backflushing [5]. The majority of former studies on fouling distribution focused on modelling work [6]. To the best of authors' knowledge, there is only one experimental study on permeate flux distribution [11]. However, this former study relied on the transmembrane pressure (TMP) measurement to analysis the permeate flux distribution. Membrane fouling can be observed by various methods, such as scanning electron microscopy (SEM) [7]. However this ex situ examination is invasive. The

membrane module needs to be destructed for SEM analysis. Hence, the fouling layer could be destroyed during sample preparation and handling. Furthermore, SEM analysis can only be performed after the filtration experiment. Direct microscopic observation method (DO) allows in situ and non-invasive visualization of the membrane surface in real-time. DO technique involves the use of an optical microscope and a camera to observe the development of membrane fouling. This technique had been used in various studies in microfiltration and ultrafiltration processes, such as alginate fouling [7], membrane backwashing [8] and microalgae deposition [9] as well as in forward osmosis process [10]. However, it has not been used to visualize the fouling distribution progress along hollow fiber membranes.

This study involved the use of an optical microscope to observe particle deposition along a hollow fiber membrane with bentonite as model foulant. The study was aimed to provide better understanding of fouling distribution along the hollow fiber membrane which would help to improve the membrane module design and the development of fouling control strategies.

2 Materials and Methods

2.1 Materials

Bentonite particles (ECP ltd) in deionized water were used as model foulants to simulate activated sludge. The size distribution of bentonite particles was measured by Master-sizer 2000. It was reported that bentonite particles could swell in water, therefore, this effect was examined by leaving the bentonite solution overnight. The particle size was then measured and compared with freshly prepared bentonite solution. Results showed that there was no significant difference in bentonite sizes. Furthermore, the filtration experiment was performed for a relatively short period of time (up to 5 hours). Hence, the particle size of bentonite should not change during experiment.

The membranes used in this study were ultrafiltration hollow fiber membranes manufactured by *Mann+Hummel*. The specifications of the membranes can be seen in Table 1.

Table 1. Specifications of hollow fiber membrane.

Material:	polyacrylonitrile (PAN)
Inner diameter:	1 mm
Outer diameter:	2 mm
Nominal pore size:	50 nm

2.2 Experimental setup

The experimental setup used in this study is shown in Figure 2 and the cross flow membrane filtration channel is shown in Figure 3. The rectangular membrane flow channels were made of glass tubes with three different lengths of 155, 305 and 505 mm. The inner dimensions of rectangular cross-section were 30 mm in width × 4 mm in height. One hollow fiber membrane was placed in the middle of the glass tube and fixed with epoxy glue. The permeate was withdrawn from one end of the fiber by using a peristaltic pump (Gilson, Minipuls 3), while the other end of the fiber was sealed. Circulation of a feed solution through the filtration channel was performed by a gear pump (Cole-Palmer). The retentate was recirculated back to the feed tank. The feed tank was equipped with a magnetic stirrer to avoid particle settlement.

Three pressure transducers (Cole-Palmer) were used to measure the transmembrane pressure (two pressure transducers installed on the feed side and one on the permeate side of the membrane). A precision balance (Sartorius) was used to record the permeate flux. The pressure transducers and the balance were connected to LabVIEW data acquisition system.

The development of membrane fouling layer was observed by an optical microscope (Nikon, Eclipse Ni-U) with 10x magnification and a color digital camera (Sony DSC-W630) with an optical zoom set at 1.2, at certain time interval and at three different locations along the hollow fiber membrane: near the suction point, in the middle of the membrane and near the sealed end. Further details of the image recording and analysis are discussed in section 2.4.

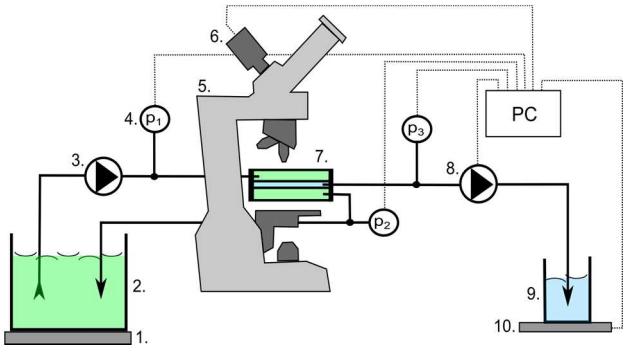

Fig. 2. The diagram of the experimental setup (1. Magnetic stirrer, 2. Beaker for bentonite solution, 3. gear pump, 4. Pressure transducers, 5. Optical microscope, 6. Digital camera, 7. Cross-flow filtration channel equipped with a hollow fiber membrane, 8. Peristaltic pump, 9. Beaker for permeate, 10. Digital balance).

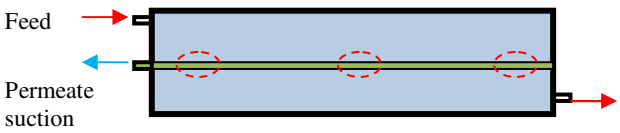

Fig. 3. The cross-flow filtration channel, depicting the feed flow, permeate suction point and the locations of fouling observation

2.3 Filtration experiments and cleaning

Filtration experiments were performed with 300 mg/L bentonite solution as feed at constant permeate flux for up to 5 hours, while the increase in suction pressure was recorded throughout the experiment. The room temperature was approximately 22°C. Various parameters were studied, these included fiber lengths (15 cm to 50 cm), cross flow velocity (18 mm/s and 33 mm/s), permeate flux (35 – 60 L m^{-2} h^{-1}). The transmembrane pressure (TMP) and the thickness of fouling layer during filtration were measured.

After each experiment, the membrane was backwashed for 20 minutes by circulating deionized water in reverse direction (inside-out) at cross flow velocity greater than 50 mm/s. The deionized waterwas then changed to 0.5% HCl and the filtration was run for the next 20 minutes. After that, the system was rinsed by running the filtration for another 20 minutes with deionized water as feed. The membrane was then ready to be re-used for the next experiment.

Transmembrane pressure (TMP) was calculated according to formula:

$$TMP = \frac{p_1+p_2}{2} - P_3\ [kPa]. \quad (1)$$

where P_2 is feed pressure, P_2 is retentate pressure and P_3 is permeate pressure.

The effective hollow fiber membrane area was calculated as below:

$$A = d \cdot \pi \cdot L\ [m^2]. \quad (2)$$

where d is the outer fiber diameter and L is the fiber length.

Cross-flow velocity was calculated from feed flow rate [m^3/s] divided by the cross-sectional area of the flow channel (width x height of the rectangular glass tube).

2.4 Image analysis

The thickness of a fouling layer along the fiber h(x, t) was measured optically with the help of visualization and image analysis. Images were taken at 3 locations along the hollow fiber membrane equally spread from the suction point to the sealed end (x = 0, 0.5L and L). All 3 pictures were taken every 20 minutes throughout the filtration experiment.

The recorded images were processed with ImageJ software and Meazure software [12-13]. All pictures were uploaded onto the software and automatically processed with help of a macro. The macro was written to speed up the image analysis process. Firstly, the color images were converted to 8 bit grey scale images. Then an evaluative rectangle was created in the middle of the picture. The dimensions of the rectangle were determined with default width of 50 pixels and default length of the same as the width of the picture (Figure 4). The mean grey value along the evaluative rectangle was calculated. This was carried out to avoid a statistical error and it resulted in a smoother curve. The curve of the mean grey value along the evaluative rectangle is shown in Figure 5. The red line connecting the gap on the curve in Figure 5 indicated the thickness of the fouling layer.

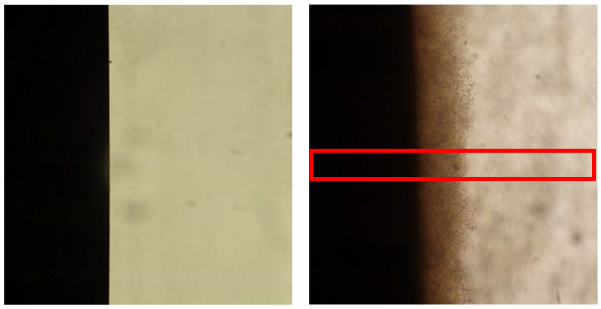

Fig. 4. Images from the digital camera of the clean hollow fiber membrane and after 1 hour of filtration (10x magnification lens).

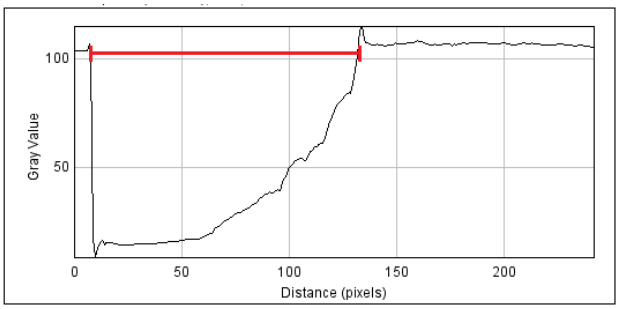

Fig. 5. Curve of the mean digital grey value along the yellow evaluative rectangle.

A scale was used to estimate the actual fouling layer thickness of an object (H_o) in [µm] as follow:

$$H_o = \frac{1}{\frac{S}{h_{i\_px}}}\ [\mu m]. \quad (3)$$

where S [px/µm] is scale of the image and hi_px is height of the object expressed as a number of pixels in the image. S was calculated from number of pixels npx, which represented 1 mm height of a scaled object (micro-ruler with 0.1 mm precision scale was used in this study).

$$S = \frac{n_{px}}{1000}\ [px/\mu m]. \quad (4)$$

Data from ImageJ were uploaded by Matlab. A threshold was set to measure the width of the gap. The same threshold was used for all images. Hence, the contrast of all images was also the same. The width of the gap in pixels was then obtained and transformed to micrometers with the help of scale S according to equation (4). For each picture, one value of thickness was calculated, which means 3 values of thickness along the hollow fiber membrane at certain time t. Since the fouling layer was developed on top of the membrane, the thickness of fouling layer was determined by subtracting the thickness of the membrane from the total thickness. The accuracy of the software in detecting the fouling layer was verified by manual measurements.

The thickness h(x, t) was expressed as cumulative distribution function (CDF) of the deposit CDFd(t) at

time t. The uniformity of the fouling layer thickness was indicated as an area A_{CDF} between CDF of the observed real fouling layer CDFd and CDF of an ideal uniform layer (Figure 6). The smaller the A_{CDF} indicated the more uniform the fouling layer thickness (hence, uniform flux distribution) along the fiber (more efficient filtration). The uniformity coefficient U [%] was calculated by using an expression shown in Figure 6.
The purpose of the measurements was to determine optimum permeate flux J and fiber length L to achieve uniform flux distribution.

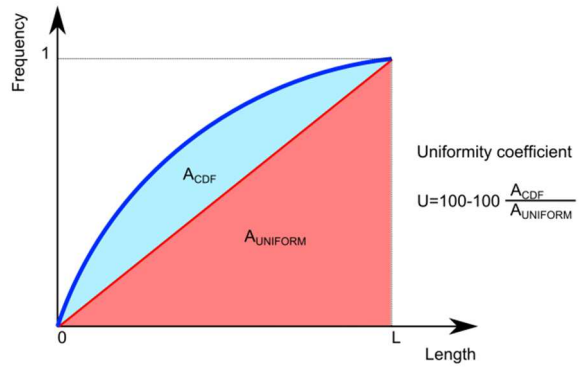

Fig. 6. CDF of the uniform layer (in red) and the real fouling layer (in blue).

3 Results and discussion

3.1 Fouling distribution along hollow fiber membrane

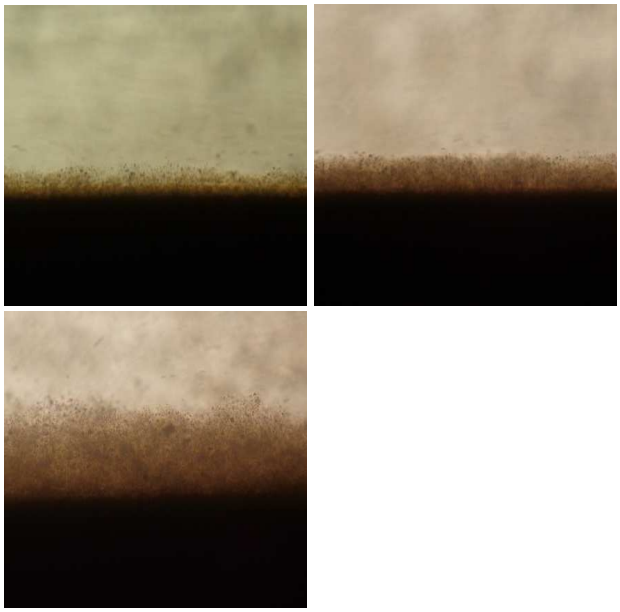

Fig. 7. Images captured at the beginning, in the middle and at the end of the 15 cm hollow fiber membrane after 1 hour of filtration and 33 mm/s CFV.

Figure 7 shows the formation of fouling layer on the membrane surface at three different locations: near the suction point, in the middle of the fiber and near the sealed end of the fiber. The images were captured at the same time after one hour of filtration. It can be seen that the cake deposition along the hollow fiber was not uniform. The fouling layer near the permeate suction point was thinner as compared to the downstream of the fiber. By referring to figure 3, the feed solution inlet was situated close to the permeate suction point (at the beginning of a fiber). Hence, the CFV was the highest at this region. Higher cross-flow shear in this region reduced the cake deposition on the membrane.

The growth of fouling layer over time can be seen in Figure 8. The images were captured near the sealed end of the fiber. It can be seen that fouling layer started to develop within the first 20 minutes of the filtration. The layer became thicker over time. The thickness of fouling layer was measured via image analysis software as described earlier and plotted in figures 9 and 10.

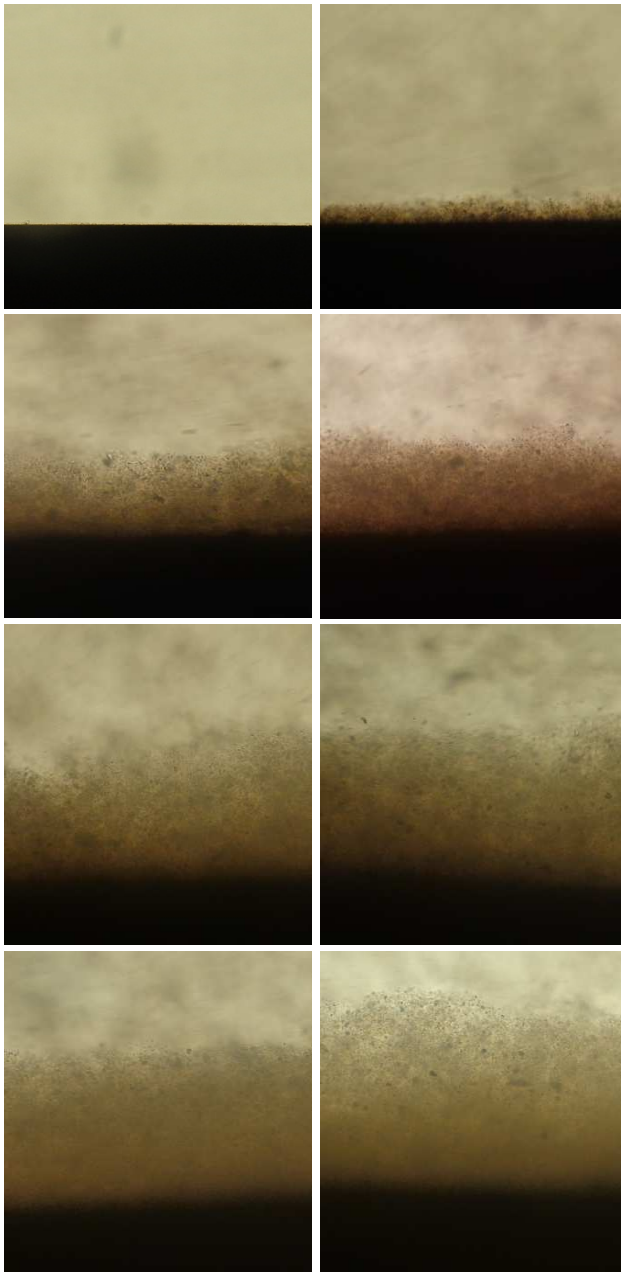

Fig. 8. Growth of fouling layer near the sealed end of the 15 cm hollow fiber membrane (images were taken at 20 minutes interval, the first image was taken at t = 0, while the last image was captured at t = 160 minutes).

At higher CFV (33 mm/sec), the cake at the beginning of a hollow fiber membrane was the thinnest (Figure 9). Interestingly, an opposite trend occurred at low CFV (18 mm/sec), the cake was the thickest near the suction point (at the beginning of the fiber) (Figure 10). As explained earlier, higher CFV near the suction point generated higher shear that helped to reduce the development of fouling layer in this region. When the CFV was decreased to 18 mm/s, fouling became more severe. At the location near the suction point, the cake buildup rapidly. After 3 hours of experiment, the cake buildup reached a plateau (Figure 10). At the beginning of experiment, the hollow fiber membrane was clean. Hence, there was more area for deposition. Once the available filtration area reduced, the rate of deposition decreased. In addition to this, although the permeate was maintained constant, the pump could not cope when the fouling became too severe. The decrease in permeate pump capacity resulted in the decreased in permeate flux, therefore, the fouling rate reduced. The filtration had to be terminated beyond this point as constant permeate flux could no longer be maintained.

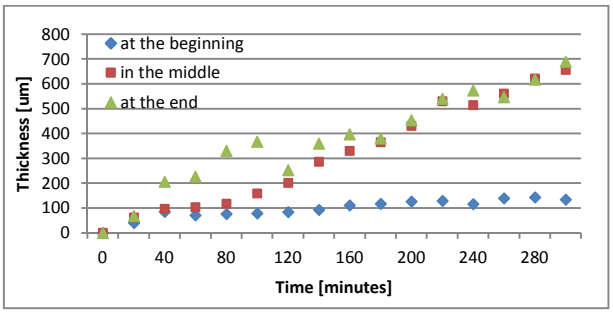

Fig. 9. Comparison of fouling layer thickness at different locations along a hollow fiber membrane vs time (15 cm fiber length, CFV 33 mm/s).

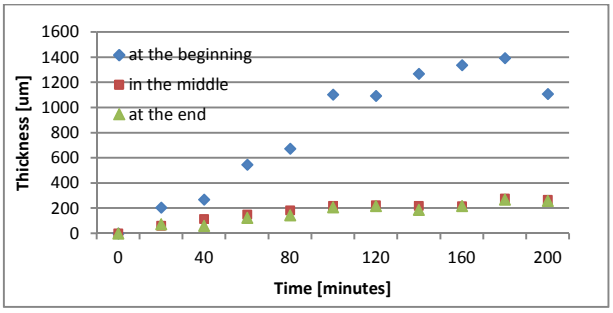

Fig. 10. Comparison of fouling layer thickness at different locations along a hollow fiber membrane vs time (50 cm fiber length, CFV 18 mm/s).

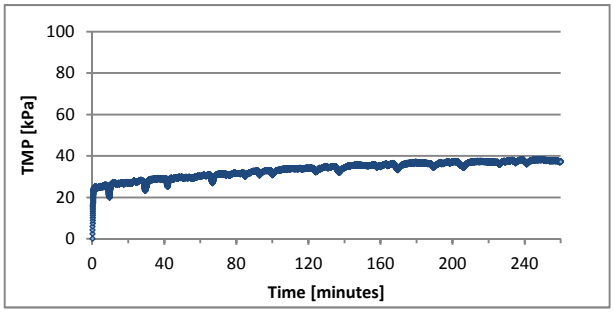

Fig. 11. TMP vs time (15 cm hollow fiber membrane, 60 LMH, CFV 33 mm/s).

The TMP profile vs time is shown in Figure 11. As expected, the TMP increased as fouling progressed. However, the TMP measurement could only reflect the severity of fouling. It could not indicate how the fouling distributed along the hollow fiber membrane. This detailed information could only be achieved by online microscopy observation method.

3.2 Effect of permeate flux

The 15 cm and 50 cm long hollow fiber membranes were tested in different permeate fluxes J = 35 LMH and 60 LMH. The trans-membrane pressure TMP(t) and thickness h(x, t) of the deposition along the hollow fiber membrane were measured during 4 hours of experiment. A uniformity coefficient U [%] of the fouling layer was calculated based on the fouling layer thickness h(x) along the fiber at time t.

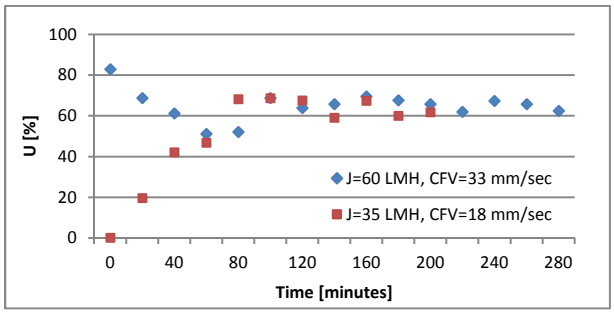

Fig. 12. Uniformity of fouling layer distribution a long hollow fiber membrane vs time at various CFV and permeate flux values (15 fiber length).

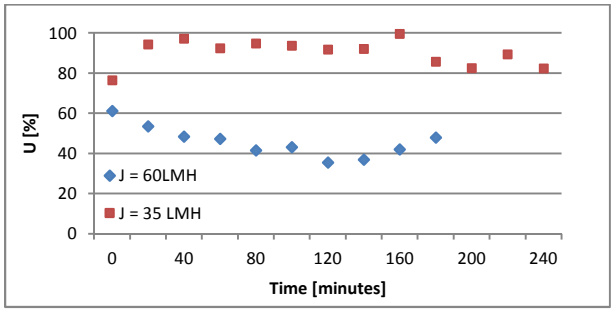

Fig. 13. Uniformity of fouling layer distribution a long hollow fiber membrane vs time at various permeate flux values (50 cm fiber length, 18 mm/s CFV).

Figure 12 represents U vs time t for different fluxes and CFVs. For filtration at higher flux and higher CFV (60 LMH and 33 mm/s, respectively), the uniformity coefficient was high at the start of the experiment which represented uniform flux distribution (the blue curve). The uniformity was decreasing over time because of fouling. Different situation was seen at lower flux and CFV (the red curve). Due to the absence of strong CFV, the non-uniformity of flux distribution developed as soon as the filtration started, with the location near the permeate suction point experienced more severe fouling. However, the uniformity of flux distribution increased over time. Once the upstream of the hollow fiber was fully covered by the cake, the permeability of this membrane section dropped, the permeate was then shifted

downstream approaching the cleaner section of the membrane. Hence, the fouling distributed more evenly along the fiber. The uniformity coefficients of both cases (red and blue curves) were relatively stable over the remaining 2 hours of experiments.
Figure 13 depicts uniformity of flux distribution as a function of time for different permeate fluxes. It can be seen that filtration at lower flux resulted in more uniform flux distribution as compared to the one at higher flux. This was due to less severe fouling occurred at lower flux. Hence, the flux distributed more evenly along the fiber. Fouling pattern mirrored the TMP and flux distribution patterns along a hollow fiber membrane.

3.3 Effect of crossflow velocity

Two different CFVs were studied for 50 cm long hollow fiber membrane. Figure 14 shows a significant difference in uniformity of filtration at low and high CFV values. Higher CFV generated higher shear-induced particle removal. Hence, the flux distributed more evenly for operation under high CFV.

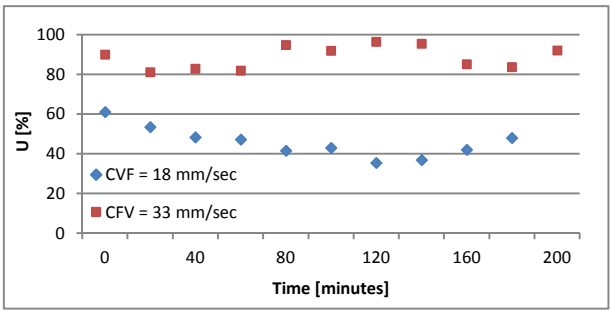

Fig. 14. Uniformity of fouling layer distribution a long hollow fiber membrane vs time at various CFV values (50 cm fiber length, 60 LMH permeate flux).

4 Conclusion

Direct microscopic observation method could provide better understanding of how fouling distributed along a hollow fiber membrane under various conditions. The image analysis method had been successfully developed to accurately measure the thickness of fouling layer. Results from this studies indicated that the flux distribution was affected by the permeate flux and cross flow velocity. Lower CFV and higher flux caused the flux to be more non-uniformly distributed due to more severe fouling. These findings provided useful information to further improve the membrane module design to achieve more evenly distributed permeate flux.

Acknowledgments

This work was supported by the Ministry of Education, Youth and Sports of the Czech Republic and the European Union - European Structural and Investment Funds in the frames of Operational Programme Research, Development and Education - project Hybrid Materials for Hierarchical Structures (HyHi, Reg. No. CZ.02.1.01/0.0/0.0/16_019/0000843).

These studies were carried out in Membrane Research Group, Department of Chemical and Materials Engineering, University of Auckland, New Zealand.

References

1. Sparks T, Chase G, Section 4 - Solid–Liquid Filtration - Filters and Filtration Handbook (Sixth Edition), Butterworth-Heinemann 2016, pp. 199-295, ISBN 9780080993966.
2. Qaisrani, T. M., Samhaber, W. M. Impact of gas bubbling and backflushing on fouling control and membrane cleaning (2011) Desalination, 266 (1-3), pp. 154-161.
3. T. Carroll, N. A. Booker. Axial features in the fouling of hollow-fibre membranes. Journal of Membrane Science 168 (2000) 203 – 212.
4. S. Chang, A. G. Fane. The effect of fibre diameter on filtration and flux distribution – relevance to submerged hollow fibre modules. Journal of Membrane Science 184 (2001) 221 – 231.
5. J. Wang, Z. Cui, H. Jia, H. Zhang. The effect of fibre length on non-uniform and hysteresis phenomenon in hollow fibre membrane backflushing. Desalination 337 (2014) 98 – 108.
6. Wang, Z., Su, K., Shu, T., Wang, W. Numerical simulation of filtration performance in submerged membrane bioreactors: Effect of particle packed structure (2017). Water Science and Technology. 76 (9). pp. 2503-2514.
7. P. Le-Clech, Y. Marselina, Y. Ye, R. M. Stuetz, V. Chen. Visualisation of polysaccharide fouling on microporous membrane using different characterization techniques. Journal of Membrane Science 290 (2007) 36 – 45.
8. Y. Marselina, Lifia, P. Le-Clech, R. Stuetz, V. Chen. Characterisation of membrane fouling deposition and removal by direct observation technique. Journal of Membrane Science 341 (2009) 163 – 171.
9. F. Wicaksana, A. G. Fane, P. Pongpairoj, R. Field. Microfiltration of algae (Chlorella sorokiniana): Critical flux, fouling and transmission. Journal of Membrane Science 387 - 388 (2012) 83 – 92.
10. Y. Wang, F. Wicaksana, C. Y. Tang, A. G. Fane. Direct microscopic observation of forward osmosis membrane fouling. Environmental Science and Technology 44/18 (2010) 7102 – 7109.
11. W. Lee, W. Cheong, K. Yeon, B. Hwang, C. Lee. Correlation between local TMP distribution and bio-cake porosity on the membrane in a submerged MBR. Journal of Membrane Science 332 (2009) 50 – 55.
12. ImageJ. Image analysis software [online: 22.9.2019], URL:<http://rsbweb.nih.gov/ij/index.html>.
13. Meazure. Image analysis software [online: 22.9.2019]. URL: <http://www.cthing.com>.